Research article

Zhao Cheng, Xiaolong Zhu, Michael Galili, Lars Hagedorn Frandsen, Hao Hu, Sanshui Xiao, Jianji Dong*, Yunhong Ding*, Leif Katsuo Oxenløwe and Xinliang Zhang

Double-layer graphene on photonic crystal waveguide electro-absorption modulator with 12 GHz bandwidth

https://doi.org/10.1515/nanoph-2019-0381
Received September 21, 2019; revised November 12, 2019; accepted November 13, 2019

Abstract: Graphene has been widely used in silicon-based optical modulators for its ultra-broadband light absorption and ultrafast optoelectronic response. By incorporating graphene and slow-light silicon photonic crystal waveguide (PhCW), here we propose and experimentally demonstrate a unique double-layer graphene electro-absorption modulator in telecommunication applications. The modulator exhibits a modulation depth of 0.5 dB/μm with a bandwidth of 13.6 GHz, while graphene coverage length is only 1.2 μm in simulations. We also fabricated the graphene modulator on silicon platform, and the device achieved a modulation bandwidth at 12 GHz. The proposed graphene-PhCW modulator may have potentials in the applications of on-chip interconnections.

Keywords: photonic crystal waveguides; graphene; modulators; electro-optical devices.

***Corresponding authors: Jianji Dong,** Wuhan National Laboratory for Optoelectronics, Huazhong University of Science and Technology, 430074 Wuhan, China, e-mail: jjdong@mail.hust.edu.cn. https://orcid.org/0000-0002-1852-8650; and **Yunhong Ding,** Department of Photonics Engineering, Technical University of Denmark, DK-2800 Kongens Lyngby, Denmark, e-mail: yudin@fotonik.dtu.dk
Zhao Cheng: Wuhan National Laboratory for Optoelectronics, Huazhong University of Science and Technology, 430074 Wuhan, China; and Department of Photonics Engineering, Technical University of Denmark, DK-2800 Kongens Lyngby, Denmark
Xiaolong Zhu and Sanshui Xiao: Department of Photonics Engineering, Technical University of Denmark, DK-2800 Kongens Lyngby, Denmark; and Center for Nanostructured Graphene, Technical University of Denmark, DK-2800 Kongens Lyngby, Denmark
Michael Galili, Lars Hagedorn Frandsen, Hao Hu and Leif Katsuo Oxenløwe: Department of Photonics Engineering, Technical University of Denmark, DK-2800 Kongens Lyngby, Denmark
Xinliang Zhang: Wuhan National Laboratory for Optoelectronics, Huazhong University of Science and Technology, 430074 Wuhan, China

1 Introduction

High-speed optical communications demand large bandwidth and low power consumption in future growing data traffics. Optical intensity modulators, as important devices in converting electric signals to optical ones, ideally need to exhibit the merits of high modulation speed, large bandwidth, small footprint, low loss and ultra-low power consumption [1]. The indispensable modulator can be achieved by light absorption in waveguide or light interference after phase tuning. For instance, traditional electro-absorption modulators, like germanium-based modulators, need a reverse bias voltage on a p-i-n-like structure to obtain an imaginary part change of the material's permittivity [2], and they are mostly limited by the operation wavelength bandwidth due to their finite band gaps [2, 3]. The light interference type intensity modulators, achieved by controlling the real part of silicon permittivity to generate a phase change, are typically designed by micro-ring resonators [4, 5] or Mach-Zehnder interferometers (MZI) [6–8]. They require either a precise fabrication method or a large footprint on the chip, which restricts their integration on large scale circuits. To meet the requirement of high-speed and low-energy consumption for the next-generation communication systems, a compact integrated electro-optical modulator with a large bandwidth and modulation depth (MD) is needed.

Two-Dimensional materials, such as graphene, MXene, phosphorene, antimonene and bismuthene, have been reported as promising materials in optical communication applications [9–14]. Integrating those materials to silicon devices has been proved to be an effective way to introduce the light-matter interaction for optical devices. As a novel material, graphene has a 2D structure which is a monolayer of carbon atoms formed in honeycomb lattice. Consequently, it performs a unique energy band structure [15, 16]. Due to its special 2D structure, graphene has the merits of easy fabrication in integration [17], ultra-wide

absorption band spectrum [18], tunable Fermi level [16, 19] and high carrier mobility [20]. In the meantime, the van der Waals force between different layers of graphene can also make hybrid integrated devices without "lattice mismatch" problem. Thanks to these distinct properties, graphene has become an attractive material for electro-optical modulators [9, 21–24]. To obtain large MD, using membrane-type photonic crystal waveguide (PhCW) with slow light effect [25] is a new way to improve weak light-matter interaction with graphene in nanometer-scale devices. PhCW is a periodic structure where light is confined by a combination of in-plane photonic band gap (PBG) confinement and vertical index guiding [26]. By introducing a line defect in this periodic structure, the defects have guided modes as two types of cutoff wavelength within the PBG, which exhibit extraordinarily large group dispersion [27]. PhCW has been utilized in plenty of applications such as sensors [28], amplifiers [29], photodetectors [30] and modulators [9]. So far, PhCW has not been exploited to implement electro-absorption modulators.

Graphene modulators rely on the tuning of its Fermi level in a capacitor structure. It can be realized either by a single-layer graphene sandwiched with a semiconductor material waveguide by a dielectric material [21], or by double-layer graphene with a dielectric material introduced in between [22]. The single-layer graphene modulators need doping in semiconductor waveguide, causing a large capacitance in the RC circuit [21]. Thus, the bandwidth is limited in 1 GHz with a MD of 0.1 dB/μm. The double-layer graphene modulator with strip waveguide achieves a MD of 0.16 dB/μm while keeping the bandwidth of 1 GHz [22]. Using the amorphous silicon on top of the double-layer graphene will significantly increase the bandwidth up to 35 GHz since the two metal pads can be close to the a-Si ridge waveguide, but it still cannot reach a large MD simultaneously [31].

Here, by combining the merits of PhCW and graphene, a novel structure, graphene-Al_2O_3-graphene sandwiched stacking on the PhCW, is proposed and demonstrated. Due to the slow light enhancement in the PhCW, a large MD up to 0.5 dB/μm with a bandwidth of 13.6 GHz is theoretically predicted. We successfully fabricated the modulator obtaining a bandwidth of 12 GHz. This design can significantly increase the MD of the modulator without sacrificing the modulation speed. It also removes the doping in the waveguide which greatly simplifies the fabrication process. The proposed electro-absorption modulator may have potentials in the optical interconnects or data-center applications.

2 Mechanism, design and simulation

The schematic structure of the proposed double-layer graphene PhCW modulator is displayed in Figure 1A. It is a silicon PhCW substrate with double-layer graphene

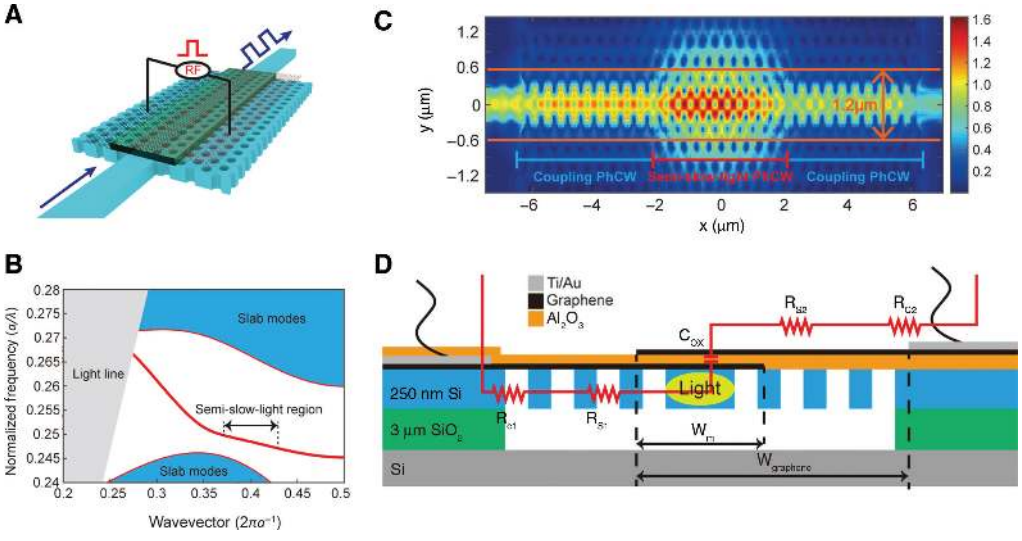

Figure 1: (A) Structure of the modulator. (B) Photonic band diagram of designed photonic crystal waveguide. (C) Electric field distribution of the PhCW. The PhCW consists of two coupling regions on each side and one semi-slow-light region in the center. The electric field extends to more than 1.2 μm in the central part. (D) Cross section of the device with equivalent RC circuit.
The parameters are pitch = 390 nm and d = 193 nm for PhCW; W_m = 1.2 μm for double-layer overlap width (not shown in scale).

separated by Al_2O_3 dielectric on the top. This graphene-oxide-graphene (G-O-G) sandwiched structure allows both electrons and holes injecting into graphene layers when a bias is applied on them. Based on the unique band dispersion of graphene, the two layers of graphene can be transparent at the same time when applied a high drive voltage, which is determined by $|E_F|$ regardless of its sign [32]. The substrate layer is a membrane silicon PhCW structure. This PhCW structure can significantly increase group index to the signal light in the defects, which serves as a larger equivalent contact area of graphene to obtain a large MD. Two Au/Ti metal pads cover on each side of the graphene to form efficient metallic contact. When a bias is applied on the two-layer graphene, the modulator will be in "ON" state for the transparent graphene. Correspondingly, the modulator will keep "OFF" state without a bias since the Fermi level of the graphene keeps at near Dirac point introducing an absorption of infrared (IR) light [33].

In order to design the PhCW, the plane-wave-expansion method [34] is used to calculate the energy band. We choose the MIT Photonic Bands (MPB) software package to compute the dispersion relationship of the PhCW. To optimize the slow-light region to be linear, we introduce some change in the W1 defect by moving the positions of the first and second rows of holes adjacent to the line defect. After optimization, we find the dispersion relationship of the PhCW in Figure 1B. Since our grating couplers are designed for transverse electric mode, we only need to consider even mode from massive guiding modes. In the end, we choose a hole diameter size of 193 nm and a lattice constant of 390 nm in our PhCW. To achieve a large group index and large bandwidth, we move the first row of holes outward from its original position for 41 nm, and the second row is moved 10 nm outward. As a result, the semi-slow-light region is linear, which is represented as the red curve in Figure 1B. Figure 1C is the electric field distribution of the PhCW, where two 5 μm coupling regions are introduced between the strip waveguide and the slow-light PhCW to reduce the coupling loss, and it indicates a good confinement of the light in the designed slow-light PhCW. The electric field is extended to a width of 1.2 μm, based on which we define the overlap width to be 1.2 μm in the later calculation. Figure 1D is the cross section of our modulator, with its equivalent circuit on it. The graphene width ($W_{grapene}$) is 3.6 μm, which is a trade-off between graphene loss and metal loss in the modulator. When a voltage is applied on the top two layers of graphene, this G-O-G structure forms a simple parallel capacitor with different doping type. The 3 dB bandwidth of the modulator can be calculated by a typical equivalent RC circuit given by

$$B = \frac{1}{2\pi[2\cdot(R_C + R_S)]\cdot C} \tag{1}$$

where R_C and R_S are the contact and sheet resistance of the graphene, respectively, and C is the capacitance of the device. To calculate the exact resistance and capacitance of the modulator, we have to decompose them into small signal electrical circuit components, shown as the red component of Figure 1D. R_C and R_S are in both sides of the cross section of the modulator, which are expressed as R_{C1}/R_{C2} and R_{S1}/R_{S2}. The capacitance is formed by the oxide layer expressed as C_{ox}

$$C = C_{ox} = \varepsilon_0\varepsilon_{Al_2O_3}\frac{W_m\cdot L}{t_{ox}} \tag{2}$$

where the t_{ox} is the thickness of the dielectric layer (aluminum oxide layer), W_m is the width of the modulation part (double-layer graphene overlap width), and L is the length of the modulator. ε_0 and $\varepsilon_{Al_2O_3}$ are the permittivity in the vacuum and Al_2O_3, respectively. We choose the contact resistance of graphene by the value of 500 Ω·μm and sheet resistance by 500 Ω/sq in our calculation [35]. The length of the modulator in simulation is set to be 5 μm, and the overlap width is 1.2 μm. Therefore, the 3 dB bandwidth of the modulator should be 13.6 GHz by putting contact resist, sheet resist to RC circuit bandwidth into Eq. (1) and capacitance thickness to Eq. (2).

In order to estimate MD and insertion loss (IL) of our design, we employ the finite-difference time-domain method through Lumerical FDTD Solution software. In the simulation setup, we use the dimensions of PhCW from previous MPB result: PhCW length of 5 μm, hole diameter of 193 nm, lattice constant of 390 nm and graphene overlap width of 1.2 μm. Before the simulation starts, we need to manually calculate the chemical potential of the graphene when a voltage is added by the following formula:

$$E_F = \mathrm{sgn}(V)\hbar v_F\sqrt{\pi\varepsilon_0\varepsilon_{Al_2O_3}|V|/t_{ox}e} \tag{3}$$

where the ħ is the reduced Planck constant, v_F is the Fermi velocity of 10^6 m/s, V is the applied voltage and e is the elementary charge. Since the two layers are in doping at same level simultaneously, we can set this value to both layers in the graphene model of this software. Figure 2A shows the transmission power of each wavelength for different voltage. The MD is the difference of output power between the zero bias and maximum corresponding to "OFF" and "ON" state. In our result, when the bias is below 4 V, the Fermi level of graphene is in the near Dirac point, as the

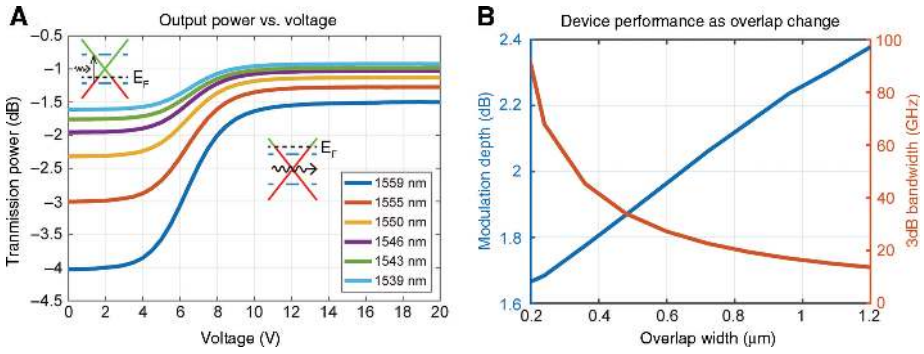

Figure 2: FDTD simulation of double-layer graphene modulator.
(A) transmission power when applied with different bias voltages; (B) modulation depth and modulation bandwidth with double-layer graphene overlap width change.

left inset in Figure 2A, which absorbs the light obviously in the "OFF" state; after increasing the bias to 10 V, the Fermi level of graphene is away from center point, which exhibits transparency property in the "ON" state. Thus, in order to obtain the maximum MD, the bias should be set between 4 V and 10 V, giving a IL between 1 dB and 1.5 dB which corresponds to 0.2–0.3 dB/μm. Thanks to the slow-light effect in the PhCW, the MD becomes larger as the wavelength increases. As is shown in Figure 2A at the wavelength of 1559 nm, the MD is up to 2.5 dB at the PhCW length of 5 μm. If we increase the length of modulator, the MD will increase at the same time.

In the modulation bandwidth and MD calculation, the overlap width (W_m) plays an important role. Figure 2B presents the MD and modulation speed as a function of overlap width. In theory, the modulation speed depends only on the overlap width regardless of the length of the modulator. However, the length of the modulator and the overlap width both affect the MD. In the end, we use the 1.2 μm overlap width for our fabricated device because it keeps a large MD and increases the fabrication tolerance, while maintaining a good modulation bandwidth.

3 Experiment and results

The details of the chip fabrication are illustrated in section 6. We firstly fabricated the PhCW, waveguides, multimode interferometer (MMI) and gratings. Buffered hydrofluoric acid is used to etch the SiO_2 layer below PhCW to make sure the PhCW is a membrane structure in low loss state. The scanning electron microscopy (SEM) image of PhCW is shown as Figure 3A. We measured the spectrum of the PhCW and MZI on the chip in Figure 3B and C before dealing with graphene. This step cannot be ignored since we need to obtain the group index and waveguide loss of PhCW. In Figure 3B, the transmission spectrum of the PhCW is the blue curve, and the red dots are group index calculated from the MZI transmission spectrum of Figure 3C. The green line is the trend of the group index, which is corresponding to the MPB simulation result in Figure 1B. The flatt area (1550–1560 nm) of green line in Figure 3B maps to the semi-slow-light region. It means that the PhCW can work in 1550 nm wavelength region with a large group index of 24. The loss of the PhCW can be calculated from the blue curve of Figure 3C, which is up to 3 dB in a waveguide length of 100 μm.

After the membranization of PhCW, the G-O-G structure is transferred and deposited on it. A 5 nm aluminum oxide layer between PhCW and bottom graphene is used to isolate silicon and graphene. The metal pad is fabricated on the graphene, which is deposited by E-beam evaporation utilizing titanium (Ti) and gold (Au), and then a lift-off process follows. The SEM image of the complete modulator is shown in Figure 4.

To measure the MD and dynamic response of the modulator, two setups are prepared, which are illustrated in section 6. When considering the measurement of MD, we aim to monitor the output power of the PhCW by applying different biases. In the beginning, we sweep the spectrum of the PhCW to find the cutoff wavelength, and then we set the tunable laser source (TLS) in the near cutoff wavelength to make sure that it is in the semi-slow light region. By manually tuning off/on the Keithly source measure unit (SMU), we record the power change in the output in order to obtain the instantaneous MD for the 10 μm long PhCW modulator, as illustrated in Figure 5A, and the MD is up to 0.55 dB, that is, 0.055 dB/μm. We further sweep the wavelength in order to achieve the wavelength-dependent MD, as shown in Figure 5B. In order to

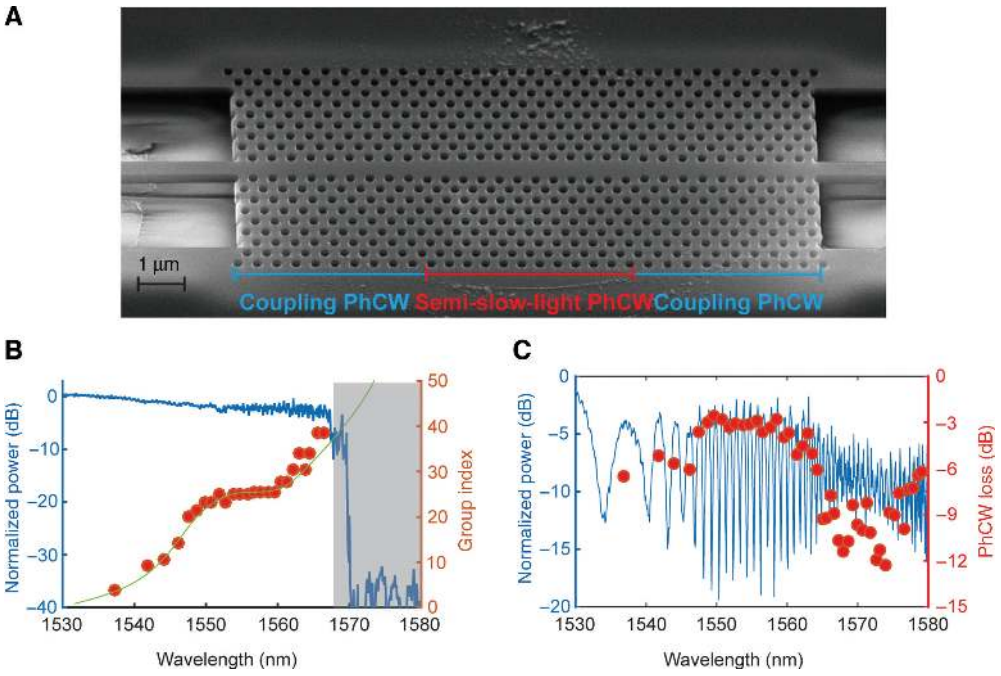

Figure 3: Characterization of the fabricated PhCW.
(A) SEM of PhCW with hole diameter of 214 nm (designed 194 nm). (B) Transmission spectrum of the PhCW (blue curve) and its group index (red dots) in each wavelength. (C) Loss (red dots) in different wavelength and spectra of the PhCW MZI (blue curve).

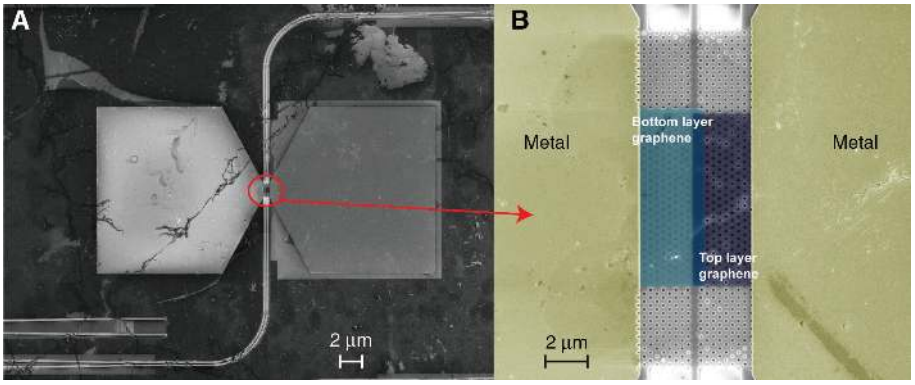

Figure 4: Characterization of the fabricate double-layer graphene modulator.
(A) SEM image of the modulator. (B) Detailed structure of the active part.

recognize the MD-wavelength tendency more easily, we choose a waveguide length of 100 μm, which exhibits a MD of 1.5 dB at 1555 nm wavelength. Those results tell us the IL and MD are dependent on wavelength, shown as Figure 5C. To measure the dynamic response of the modulator, an electrical signal generated by a vector network analyzer (VNA) is superimposed onto a static drive voltage for small signal measurement. The frequency range of VNA is set from 50 MHz to 20 GHz with a radio frequency (RF) power of 20 dBm in a static voltage of 8 V. We use the 1555 nm wavelength which is in the semi-slow light region. Figure 5D tells us the result from the VNA which illustrates the 3 dB bandwidth of the modulator is up to 12 GHz.

4 Discussion

The modulator performs a MD of 0.55 dB and modulation speed of 12 GHz in the length of 10 μm. The MD increases in longer wavelength. This phenomenon indicates that the PhCW has a larger group index in longer wavelength, and it has a trade-off result between MD and IL in semi-slow light region at nearly 1555 nm. The

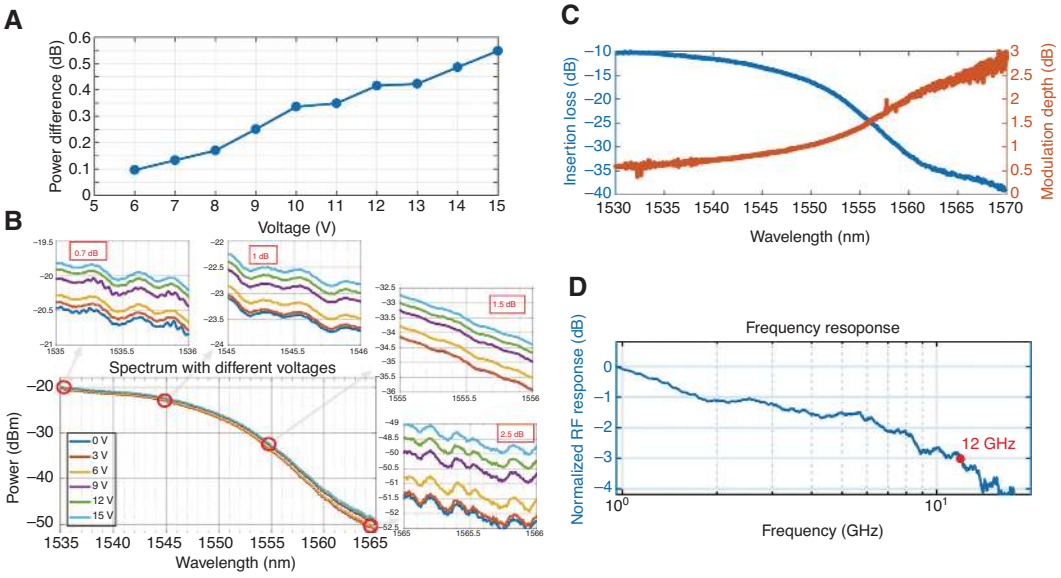

Figure 5: (A) The output power difference for a 10 μm PhCW modulator with different bias voltages. (B) Spectrum of a 100 μm PhCW modulator when applying biases (changing from 0 V to 15 V). (C) Wavelength-dependent insertion loss and modulation depth. (D) Frequency response of the modulator with DC of 8 V and RF power of 20 dBm.

IL is the same as our expectations in the simulation part. However, the MD is smaller than our simulation expectations, which is attributed to the dirty graphene layer as shown in the SEM image of the modulator in Figure 4B. Besides, we can see the top layer graphene does not cover the whole first row of the photonic crystal as we expected due to the misalignment in the lithography process. It is found from the electric field distribution in Figure 1C that the mode field is expanded to the whole first row of the PhCW. Thus, the misalignment significantly reduces the MD. The bandwidth is affected by the capacitance and resistance of the modulator from Figure 1D and Eq. (1). The capacitance of the modulator drops off a little because of the over-etched overlap length introduced by the misalignment, and the resistance increases due to the poor quality of top layer graphene. Thus, the bandwidth is limited to 12 GHz.

The misalignment problem comes from multiple lithography and atomic layer deposition (ALD) process when dealing with the bottom layer graphene and Al_2O_3. To solve the problem, we need to consider adding an additional size of graphene in E-beam lithography. It is necessary to exert effort to find the best area for lithography before O_2 plasma etching process. The poor graphene quality comes from the rough surface of Al_2O_3 thin film. To overcome it, we can also try a different thickness of Al_2O_3 to find the best performance in the interface between Al_2O_3 and graphene. On the other hand, using other 2D materials, such as phosphorene [13] and antimonene [36], may offer different solutions on the modulator. The transfer method of these materials can provide a complete pattern on the devices. However, they are not easy to transfer to massive integrated devices as far as we know.

5 Conclusion

In conclusion, we have proposed a double-layer graphene membrane type PhCW electro-absorption modulator. The theoretical simulation indicates the modulator has a MD of 0.5 dB/μm with a bandwidth of 13.6 GHz, which is 3 times larger than traditional double-layer graphene modulators. The 10 μm effective length experiment demo modulator has a 3 dB bandwidth up to 12 GHz with a MD of 0.55 dB. A 100 μm long modulator exhibits a 1.5 dB MD, which can be improved significantly with improved fabrication process. Thanks to the slow-light region of PhCW, those modulators can work in a telecommunication band for 10 nm bandwidth. Experiment results verify the MD enhancement by the PhCW. It is a promising method to achieve large bandwidth and high MD with simple fabrication process.

6 Fabrication and experiment methods

The fabrication starts with commercial silicon-on-insulator wafers (bought from Soitec, Bernin, France)

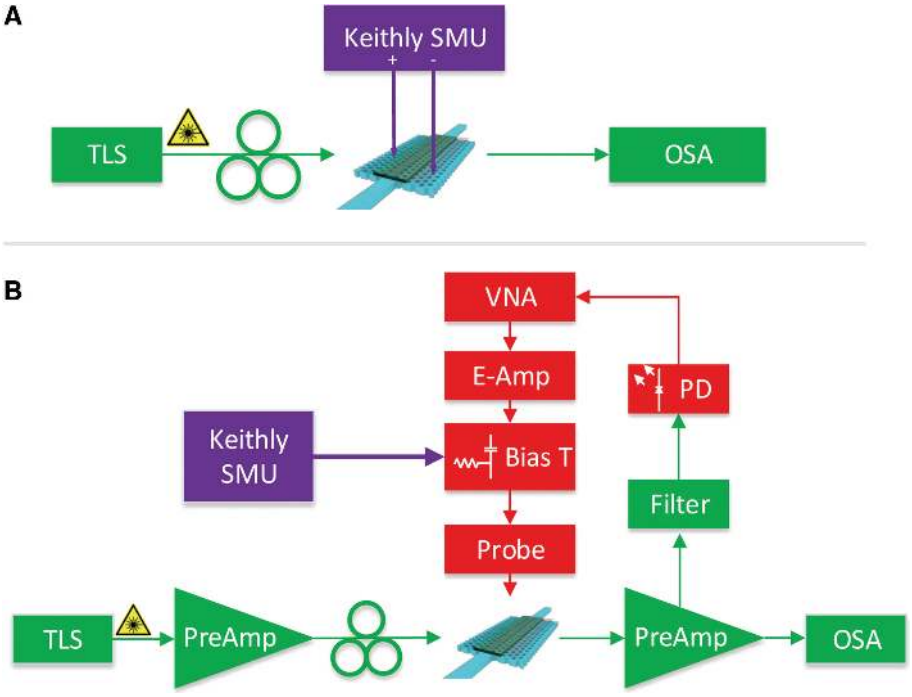

Figure 6: (A) Setup for measuring modulation depth: measuring modulation depth by changing DC source; (B) setup for measuring frequency response.
Green part is the optical circuit, red part is the RF cable and components, purple part is the DC device.

with a 250-nm-thick silicon layer on top of a 3 µm SiO_2 buried layer. E-beam lithography (JEOL JBX-9500FS, JEOL, Tokyo, Japan) and inductively coupled plasma with Bosch process (STS MESC Multiplex ICP serial no. 30343, STS, Newport, Wales, UK) are used to fabricate the PhCW, waveguides, MMI and gratings. To etch SiO_2 under the PhCW, standard ultraviolet lithography is used to define the wet etch regions by AZ5214E, which works as a mask to protect the other components like gratings, MMI and waveguides. Buffered hydrofluoric acid is used to etch the SiO_2 layer below PhCW to make sure the PhCW is a membrane structure in low losses state. The PhCW scanning electron microscopy (SEM) image is shown as Figure 3A. After the membranization, a 5 nm aluminum oxide layer is deposited on the device by ALD for isolating silicon and graphene. The bottom layer graphene is wet-transferred onto the surface from a chemical vapor deposition grown copper foil. Then, the graphene shape is defined using E-beam lithography and O_2 plasma etching. Next, the metal pad is fabricated on the graphene, which is deposited by E-beam evaporation utilizing titanium (Ti) and gold (Au), and then a lift-off process is followed. To overcome the hydrophobic nature of graphene basal plane [37], we firstly deposit 2 nm of aluminum since the trimethylaluminum/H_2O process cannot be directly deposited on the graphene. The aluminum by thermal evaporation will be immediately oxidized into Al_2O_3 when exposed to the air. Then, 28 nm of Al_2O_3 is deposited at 200°C in ALD process. A similar process is performed on the top layer of graphene as on the bottom layer.

We characterized the fabricated device at room temperature in ambient conditions. Figure 6A is the setup used to measure the MD of the modulator. A TLS (Ando, AQ4321A, Ando Electric, Kawasaki, Japan) is synchronized with optical spectrum analyser (OSA) (Ando, AQ6317B, Ando Electric, Kawasaki, Japan) to sweep the spectrum of the modulator, and then we set the TLS at the cutoff wavelength of the PhCW. By tuning off/on of the SMU (Keithly, 238), the maximum and minimum of the output power are recorded from the OSA. The maximum difference power is the MD. Moreover, we set the SMU in the voltage from 0 V to 15 V, measuring the spectrum of each specific voltage. Figure 6B is the dynamic measurement setup. Electrical signal generated by a VNA (HP, 8722C) is superimposed onto a static drive voltage for small signal measurement. The frequency range of VNA is set from 50 MHz to 20 GHz with a RF power of 20 dBm in a static voltage of 8 V. We set the TLS at 1555 nm wavelength which is in the semi-slow light region. The optical output of the device is directed into an IR photodetector (u2t photonics, XPDV2020R, 50 GHz) then guided into VNA port.

Acknowledgments: This work is supported by the Danish Council for Independent Research (No. 9041-00333B), the National Key Research and Development Project of China (2018YFB2201901), the National Natural Science Foundation of China (61622502, 61805090), the mid-chip project sponsored by VILLUM FONDEN (funder id: http://dx.doi.org/10.13039/100008398, No. 13367), the Center for Silicon Photonics for Optical Communication (SPOC) sponsored by the Danish National Research Foundation (funder id: http://dx.doi.org/10.13039/501100001732, project DNRF123) and the Center for Nanostructured Graphene (CNG) sponsored by the Danish National Research Foundation (funder id: http://dx.doi.org/10.13039/501100001732, project DNRF103). Z. C. is sponsored by the China Scholarship Council (CSC), funder id: http://dx.doi.org/10.13039/501100004543, grant number: 201706160051, to support his work in Denmark.

Conflicts of interest: There are no conflicts to declare.

References

[1] Reed GT, Mashanovich G, Gardes FY, Thomson DJ. Silicon optical modulators. Nat Photonics 2010;4:518–26.
[2] Srinivasan SA, Pantouvaki M, Gupta S, et al. 56 Gb/s germanium waveguide electro-absorption modulator. J Lightwave Technol 2016;34:419–24.
[3] Chaisakul P, Marris-Morini D, Frigerio J, et al. Integrated germanium optical interconnects on silicon substrates. Nat Photonics 2014;8:482–8.
[4] Xu Q, Manipatruni S, Schmidt B, Shakya J, Lipson M. 12.5 Gbit/s carrier-injection-based silicon micro-ring silicon modulators. Opt Express 2007;15:430–6.
[5] Yu H, Ying D, Pantouvaki M, et al. Trade-off between optical modulation amplitude and modulation bandwidth of silicon micro-ring modulators. Opt Express 2014;22:15178–89.
[6] Dong P, Chen L, Chen YK. High-speed low-voltage single-drive push-pull silicon Mach-Zehnder modulators. Opt Express 2012;20:6163–9.
[7] Green WMJ, Rooks MJ, Sekaric L, Vlasov Y. Ultra-compact, low RF power, 10 Gb/s silicon Mach-Zehnder modulator. Opt Express 2007;15:17106–13.
[8] Liao L, Samara-Rubio D, Morse M, et al. High speed silicon Mach-Zehnder modulator. Opt Express 2005;13:3129–35.
[9] Yan S, Zhu X, Frandsen LH, et al. Slow-light-enhanced energy efficiency for graphene microheaters on silicon photonic crystal waveguides. Nat Commun 2017;8:14411.
[10] Song Y, Chen Y, Jiang X, et al. Nonlinear few-layer MXene-assisted all-optical wavelength conversion at telecommunication band. Adv Opt Mater 2019;7:1801777.
[11] Wang K, Zheng J, Huang H, et al. All-optical signal processing in few-layer bismuthene coated microfiber: towards applications in optical fiber systems. Opt Express 2019;27:16798–811.
[12] Song Y, Liang Z, Jiang X, et al. Few-layer antimonene decorated microfiber: ultra-short pulse generation and all-optical thresholding with enhanced long term stability. 2D Mater 2017;4:045010.
[13] Wang Y, Zhang F, Tang X, et al. All-optical phosphorene phase modulator with enhanced stability under ambient conditions. Laser Photonics Rev 2018;12:1800016.
[14] Dai D, Yin Y, Yu L, et al. Silicon-plus photonics. Front Optoelectron 2016;9:436–49.
[15] Castro Neto AH, Guinea F, Peres NMR, Novoselov KS, Geim AK. The electronic properties of graphene. Rev Mod Phys 2009;81:109–62.
[16] Geim AK, Novoselov KS. The rise of graphene. Nat Mater 2007;6:183.
[17] He Q, Sudibya HG, Yin Z, et al. Centimeter-long and large-scale micropatterns of reduced graphene oxide films: fabrication and sensing applications. ACS Nano 2010;4:3201–8.
[18] Bao Q, Zhang H, Wang B, et al. Broadband graphene polarizer. Nat Photonics 2011;5:411.
[19] Novoselov KS, Geim AK, Morozov SV, et al. Electric field effect in atomically thin carbon films. Science 2004;306:666–9.
[20] Bolotin KI, Sikes KJ, Jiang Z, et al. Ultrahigh electron mobility in suspended graphene. Solid State Commun 2008;146:351–5.
[21] Liu M, Yin X, Ulin-Avila E, et al. A graphene-based broadband optical modulator. Nature 2011;474:64–7.
[22] Liu M, Yin XB, Zhang X. Double-layer graphene optical modulator. Nano Lett 2012;12:1482–5.
[23] Phare CT, Daniel Lee YH, Cardenas J, Lipson M. Graphene electro-optic modulator with 30 GHz bandwidth. Nat Photonics 2015;9:511–4.
[24] Koester SJ, Li M. High-speed waveguide-coupled graphene-on-graphene optical modulators. Appl Phys Lett 2012;100:171107.
[25] McNab SJ, Moll N, Vlasov YA. Ultra-low loss photonic integrated circuit with membrane-type photonic crystal waveguides. Opt Express 2003;11:2927–39.
[26] Jiang Y, Jiang W, Gu L, Chen X, Chen RT. 80-micron interaction length silicon photonic crystal waveguide modulator. Appl Phys Lett 2005;87:221105.
[27] Notomi M, Yamada K, Shinya A, Takahashi J, Takahashi C, Yokohama I. Extremely large group-velocity dispersion of line-defect waveguides in photonic crystal slabs. Phys Rev Lett 2001;87:253902.
[28] Mortensen NA, Xiao S. Slow-light enhancement of Beer-Lambert-Bouguer absorption. Appl Phys Lett 2007;90:141108.
[29] Ek S, Lunnemann P, Chen Y, Semenova E, Yvind K, Mork J. Slow-light-enhanced gain in active photonic crystal waveguides. Nat Commun 2014;5:5039.
[30] Schuler S, Schall D, Neumaier D, et al. Graphene photodetector integrated on a photonic crystal defect waveguide. ACS Photonics 2018;5:4758–63.
[31] Dalir H, Xia Y, Wang Y, Zhang X. Athermal broadband graphene optical modulator with 35 GHz speed. ACS Photonics 2016;3:1564–8.
[32] Hanson GW. Dyadic Green's functions and guided surface waves for a surface conductivity model of graphene. J Appl Phys 2008;103:064302.
[33] Mak KF, Sfeir MY, Wu Y, Lui CH, Misewich JA, Heinz TF. Measurement of the optical conductivity of graphene. Phys Rev Lett 2008;101:196405.

[34] Johnson SG, Joannopoulos JD. Block-iterative frequency-domain methods for Maxwell's equations in a planewave basis. Opt Express 2001;8:173–90.
[35] Kovacevic G, Phare C, Set SY, Lipson M, Yamashita S. Ultra-high-speed graphene optical modulator design based on tight field confinement in a slot waveguide. Appl Phys Express 2018;11:065102.
[36] Wang Y, Huang W, Wang C, et al. An all-optical, actively Q-switched fiber laser by an antimonene-based optical modulator. Laser Photonics Rev 2019;13:1800313.
[37] Lee B, Park SY, Kim HC, et al. Conformal Al2O3 dielectric layer deposited by atomic layer deposition for graphene-based nanoelectronics. Appl Phys Lett 2008;92:203102.